ARL

US Army Research Laboratory

Preferred Orientation of Rare Earth (RE)-Doped Alumina Crystallites by an Applied Magnetic Field

by Carli A Moorehead, Victoria L Blair, Krista R Limmer, Raymond E Brennan, and Jane W Adams

NOTICES

Disclaimers

The findings in this report are not to be construed as an official Department of the Army position unless so designated by other authorized documents.

Citation of manufacturer's or trade names does not constitute an official endorsement or approval of the use thereof.

Destroy this report when it is no longer needed. Do not return it to the originator.

ARL

Preferred Orientation of Rare Earth (RE)-Doped Alumina Crystallites by an Applied Magnetic Field

by Victoria L Blair, Raymond E Brennan, and Jane W Adams
Weapons and Materials Research Directorate, ARL

Carli A Moorehead
Battelle Memorial Institute, Columbus, OH

Krista R Limmer,
Oak Ridge Institute for Science and Education, Oak Ridge, TN

REPORT DOCUMENTATION PAGE

1. REPORT DATE *(DD-MM-YYYY)*	2. REPORT TYPE	3. DATES COVERED (From - To)
June 2016	Final	1 September 2015–31 January 2016

4. TITLE AND SUBTITLE

Preferred Orientation of Rare Earth (RE)-Doped Alumina Crystallites by an Applied Magnetic Field

5a. CONTRACT NUMBER

5b. GRANT NUMBER

5c. PROGRAM ELEMENT NUMBER

6. AUTHOR(S)

Carli A Moorehead, Victoria L Blair, Krista R Limmer, Raymond E Brennan, and Jane W Adams

5d. PROJECT NUMBER

DSI-14-WMR-014

5e. TASK NUMBER

5f. WORK UNIT NUMBER

7. PERFORMING ORGANIZATION NAME(S) AND ADDRESS(ES)

US Army Research Laboratory
ATTN: RDRL-WMM-E
Aberdeen Proving Ground, MD 21005-5069

8. PERFORMING ORGANIZATION REPORT NUMBER

ARL-TR-7702

9. SPONSORING/MONITORING AGENCY NAME(S) AND ADDRESS(ES)

10. SPONSOR/MONITOR'S ACRONYM(S)

11. SPONSOR/MONITOR'S REPORT NUMBER(S)

12. DISTRIBUTION/AVAILABILITY STATEMENT

Approved for public release; distribution is unlimited.

13. SUPPLEMENTARY NOTES

14. ABSTRACT

Alumina (aluminum oxide, Al_2O_3) has many favorable properties but is challenging to make transparent because of its anisotropic crystal structure. To combat the anisotropy, magnetic alignment of the particles can be used to minimize the change in index of refraction from grain to grain, thus reducing light scattering and allowing for transparency. Density functional theory results indicated that adding a rare-earth (RE) dopant enhanced the magnetic anisotropy of the alumina crystals, making them more responsive to a magnetic field. Further, different RE dopants were predicted to induce various degrees of magnetic moment localization and affect the orientation of the magnetic easy axis. It is of interest to investigate what effect the identity of the dopant has on the response to the magnetic field. RE dopants praesodymium, gadolinium (Gd), ytterbium (Yb), and erbium were used to dope nano-sized alumina powders, which were then suspended in epoxy resin that was allowed to cure within a magnetic field. The micro-texture of the aligned ceramic was analyzed by X-ray diffraction and the Lotgering factor calculated. $Gd:Al_2O_3$ was found to have approximately the same response as $Yb:Al_2O_3$ despite inducing different magnetic moments.

15. SUBJECT TERMS

grain alignment, micro-texture, magnetic field processing, transparent ceramics, laser ceramics

16. SECURITY CLASSIFICATION OF:			17. LIMITATION OF ABSTRACT	18. NUMBER OF PAGES	19a. NAME OF RESPONSIBLE PERSON
a. REPORT	**b. ABSTRACT**	**c. THIS PAGE**			Carli A Moorehead
Unclassified	Unclassified	Unclassified	UU	28	**19b. TELEPHONE NUMBER (Include area code)** 410-306-4947

Contents

List of Figures

List of Tables

Acknowledgments

INTENTIONALLY LEFT BLANK.

1.   Introduction

Transparent, polycrystalline ceramics are vital to applications such as transparent armor, laser host materials, and optical sensing. However, transparent ceramics have been limited to those materials with isotropic unit cells as either single crystals or nanocrystalline polycrystals.[1–3] Anisotropic ceramics can only be made transparent in the nanocrystalline polycrystal form when the nanocrystals are smaller than the wavelength of light.[1–3] To obtain transparent ceramics, 2 requirements must be met: 1) the material cannot absorb or reflect light, and 2) the material cannot substantially scatter light.[1–4] While most technical ceramics do not absorb a significant amount of light, most scatter light for a number of reasons, as shown in Fig. 1. Scattering occurs when there is an interface between 2 media with different refractive indices.[1] Optical inhomogenities such as second phases, contaminants, and pores, in particular, have different indices of refraction, causing light to be refracted and/or reflected at the interface.[1–4] Additionally, grain boundaries in anisotropic ceramics cause scattering because different crystal planes have slightly different refractive indexes; when grains are randomly oriented, light is scattered as it passes from grain to grain.[1] In order for a sample to be transparent, these scattering centers have to be either much bigger or much smaller than the wavelength of light passing through the sample.[1–3] Since the visual spectrum of light is between 400 and 700 nm (~0.5 μm), grains must either be much larger (several hundred microns) or much smaller (tens of nanometers).
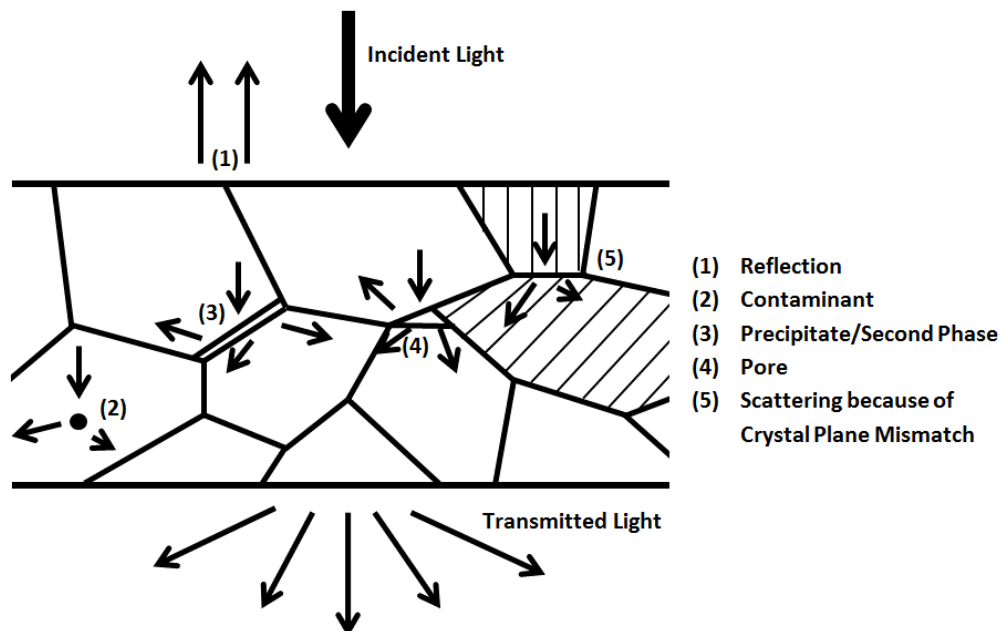

Fig. 1   Sources of light scattering in polycrystalline ceramics

Since large, single crystals are difficult and costly to produce, there are 2 distinct approaches to producing transparent anisotropic, polycrystalline ceramics such as alumina: 1) minimize grain size or 2) enhance grain orientation. The former has been used frequently to produce transparent ceramics, while the latter has not.[1–5] For grain orientation (crystallographic texture) to be used alone, it has been theorized that all grains would have to be perfectly aligned, thereby essentially behaving as a single crystal.[1] Since that is an unlikely solution, a third, hybrid approach to producing transparent ceramics has been identified: minimizing grain size while simultaneously enhancing grain alignment. Since transparency is being optimized in 2 different ways, it is theorized transparency will be observed for grains of moderate size (~600 nm) under moderate alignment (70%–80%), thus significantly altering the processing route and alleviating the need to produce either extreme.[1]

Methods for producing fine ceramic powders with homogenous final sintered microstructures have been extensively explored, since fine grains lead to advantageous mechanical properties and transparency.[6] A method for producing nano-sized alumina powder by a co-precipitation process has already been established.[7,8] In this method, aluminum nitrate along with nitrates of any preferred dopants are dissolved in water and added drop-wise with a basic ammonium bicarbonate solution into a buffer solution. An aluminum-ammonium-carbonated-hydrate results, forming nano-grained alumina with a high surface area upon calcination.

Several techniques have been explored to produce grain alignment. They include platelet seeding for templated grain growth, hot pressing, tape casting platelets, incorporating sintering additives, and magnetic alignment, the last of which has not been well researched.[5,9–19] Magnetic manipulation of liquid metals has been used for some applications, but those techniques are of limited use in ceramics due to the inherently low magnetic susceptibility of ceramics and the high viscosity of the system due to significantly higher melting temperatures of ceramics.[11,18,20,21] Ceramics are often paramagnetic or diamagnetic and therefore have typically low magnetic susceptibilities.[10,11,13,14,17] Magnetic susceptibility is a measure of how strongly a material will magnetize in response to an applied magnetic field and consequently is also a measure of how strong a field will be necessary to get an appreciable response.[22] Furthermore, many ceramics exhibit magnetic susceptibility anisotropy due to different magnetic susceptibilities associated with different crystallographic directions.[11–14,17,19,21] Because of this anisotropy, such crystals will align the axis with the highest magnetic susceptibility in the direction of the field providing a potential mechanism for preferred crystal orientation in diamagnetic materials.[11–14,17,19,21] The magnetic response of ceramics is governed

by 2 main equations. Equation 1 describes the anisotropic magnetic energy (ΔE) as a function of the system properties and the applied magnetic field. Equation 2 describes the temporal requirement (t) for rotating the crystal assuming no steric hindrance.[23]

$$\Delta E = V \frac{(\chi_c - \chi_{a,b})B^2}{\mu_0} > k_B T ,$$ (1)

and

$$t = -\mu_0 \frac{30\eta + r^2 \sigma B^2}{5(\chi_c - \chi_{a,b})B^2} ln \left(\frac{tan\Theta}{tan\Theta_0} \right) ,$$ (2)

where V is the primary crystal volume, $\chi_{a,b}$, and χ_c are the magnetic susceptibilities of the crystallographic planes that will be perpendicular and parallel to the magnetic field, respectively, following alignment, μ_0 is the permeability of free space, B is the externally imposed magnetic flux density, k_B is Boltzmann's constant, T is the absolute temperature, t is the time needed for a crystal to rotate a certain amount assuming no steric hindrances, η is the viscosity of the melt or fluid surrounding the crystal, r is the crystallite radius, σ is the electrical conductivity of the particle, and Θ_0 and Θ are, respectively, the initial and final angles of the crystal easy-axis (parallel axis, χ_c) with respect to the magnetic field.[23]

In order for alignment to occur, the magnetic energy on a crystal inciting rotation must be larger than the thermal energy ($k_b T$), Eq. 1.[23] Additionally, the magnetic energy is a function of 3 variables demonstrated in Fig. 2: first, the crystal size, second, the difference in magnetic susceptibility across different crystallographic planes, and finally, the magnetic field strength. Furthermore, there is a time dependence on magnetic alignment based on the environment around the particles and their own magnetic energy. From Eq. 2 it is evident that this is a function of the viscosity of the fluid phase,[19] particle conductivity, the degree of rotation necessary, and the magnetic energy of the crystals. Based on those factors, it is anticipated that an extremely strong magnetic field on the order of several tesla will be necessary to produce the required magnetic torque for achieving magnetic alignment in nano-sized crystallites of a material with weak magnetic susceptibility anisotropy.[17,24] Additionally, it is imperative to use a ceramic forming system with a low viscosity liquid phase. For that reason, almost all magnetic alignment studies of ceramic particles involve some form of colloidal processing; slip-casting, gel-casting, or tape casting, which gives particles the mobility of a low-viscosity liquid phase in the absence of a melt.[5,9,12–15,17,19]
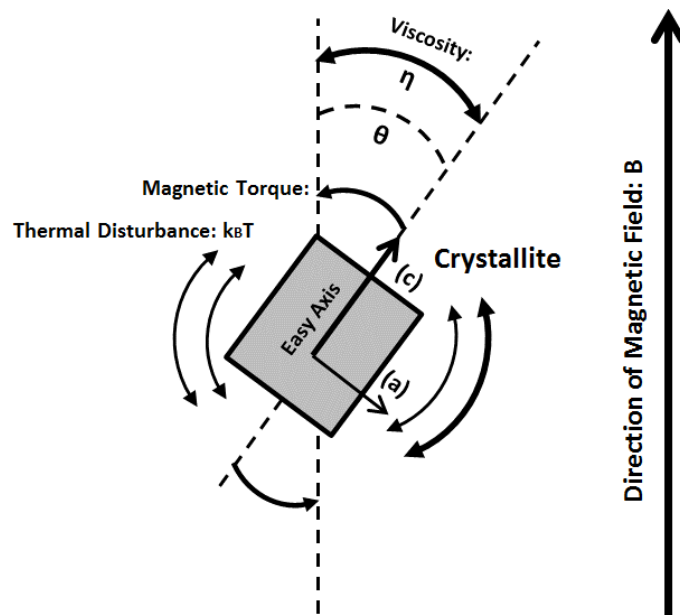
Fig. 2   Schematic illustrating Eq. 1 showing the forces acting on a weak magnetic crystallite in a magnetic field

Alumina's favorable thermal properties make it an excellent choice for a laser host media, aside from being optically anisotropic. However, this anisotropy may be overcome using the hybrid approach of both minimizing grain size and maximizing grain alignment. Including rare-earth (RE) dopants should allow alumina to lase and enhance the magnetic susceptibility of the alumina for increased grain alignment under a magnetic field. In this study, the effect of RE dopants on the grain alignment of alumina was considered to determine which RE dopants provide the greatest response and to determine their efficacy at enhancing grain alignment. Nano-sized alumina particles were suspended in an epoxy at low-solids loading and set under an applied magnetic field before being analyzed with X-ray diffraction (XRD) to determine the grain alignment. Density functional theory (DFT) calculations were performed to aid in understanding the source of the RE dopant effects. The results of this study enable development of a gel-casting system for oriented green bodies, eventual sintering, and producing high-quality transparent parts.

2.   Methods and Materials

2.1 Synthesis of Nano-Alumina Ceramic Powders

A co-precipitation method was used to synthesize amorphous pre-alumina powder in an aqueous environment.[8] Prior to precipitation, 2 solutions were prepared: an

acidic solution (solution A) and a basic solution (solution B). The acidic solution consisted of aluminum nitrate, magnesium nitrate, and RE nitrate in stoichiometric amounts to get a composition of $RE_xAl_{2-x}O_3$ (RE = Er [erbium], Pr [praseodymium], Gd [gadolinium], Yb [ytterbium], 400 ppm) and 250 ppm of magnesium. Adding magnesium to alumina had the dual purpose of creating structural distortion to assist in dissolving the RE into the Al octahedral site and acting as a grain growth inhibitor.[25] Deionized (DI) water was added to the mixed nitrates to get a 7.5-M solution of $Al(NO_3)_3$; the RE and magnesium nitrates were not included in the calculation. The basic solution consisted of 11% by weight ammonium bicarbonate and 3% by weight ammonium hydroxide in DI water. Both solutions were stirred until all crystals had dissolved, adding heat if necessary.

Once solutions A and B were prepared, a third buffer solution was mixed in which the reactions would take place. The amount of buffer solution (2% by weight ammonium bicarbonate in DI water) depended on the batch size. The pH of the buffer solution was adjusted to approximately 7 with a small amount of nitric acid. Finally, solutions A and B were added drop-wise to the buffer solution in such a way that the pH stayed at approximately 7 during the entire precipitation exercise. When solution A was exhausted and the pH remained stable at approximately 7, the resulting suspension was allowed to age while stirring vigorously, overnight. Following aging for greater than 12 h, the suspension was filtered from the salty solution. The resulting powder was then washed twice with DI water and once with isopropyl alcohol. After washing, the powder was put into an oven to dry. The dry powder was gently crushed and calcined at 1,300 °C for 30 min (10 °C/min heating and cooling rate).

2.2 Magnetic Alignment Studies

Two-part, room-temperature curing epoxy (EP1112NC Clear, Resinlab, Germantown, WI) was used to suspend powder and hold it in place after alignment. First, alumina/methanol slurries were ball milled to break up agglomerates generated from the calcination process. After ball milling, the alumina/methanol slurry was added to Part A of the epoxy and mixed using a wrist action shaker. Methanol was used as the solvent because it could be used to dilute the epoxy without changing the overall properties of the epoxy, allowing for thorough mixing of the alumina in the epoxy. Enough alumina/methanol slurry was added to Part A so that the final ratio of alumina to cured epoxy would yield 20 wt%. Finally, the methanol was evaporated out of Part A in a hot water bath resulting in an alumina powder suspended in Part A epoxy. On the date of magnetic alignment, the alumina/Part A suspension was added to the calculated amount of Part B for curing. The parts were mixed well with a wooden stir stick, cast into lubricated 1-inch

cylindrical plastic potting cups, and set under no-field (control), 1.8-T magnetic field (1.8-T electromagnet, Fig. 3), and 9-T magnetic field (9-T Horizontal Bore Superconducting Magnetic, American Magnetics Inc., Oak Ridge, TN). After sitting in the field for at least 3 h, a heat gun was used to accelerating the epoxy curing process during the control and 1.8-T conditions. The samples cured at 9 T were allowed to cure at room temperature overnight.
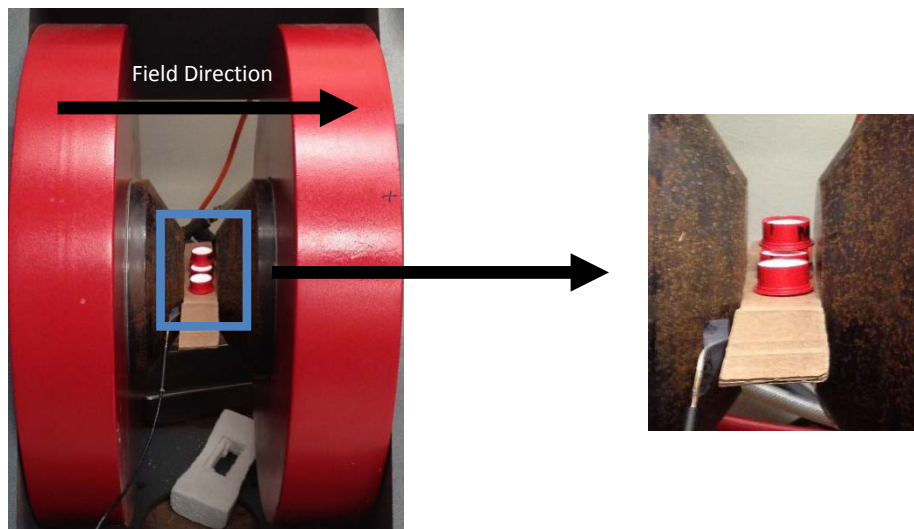
Fig. 3   Aligning epoxy and slurry casts within a 1.8-T magnetic field

After curing, the pucks were demolded, cut parallel to the field direction, and cross-sectioned as shown in Fig. 4, for analysis with XRD using Cu-Kα radiation at 30 kV, 15 mA (Rigaku MiniFlex II). XRD scans were performed over a 34–45 °2θ range, at a step angle of 0.01 °2θ, and a scan rate of 1 °2θ/min.
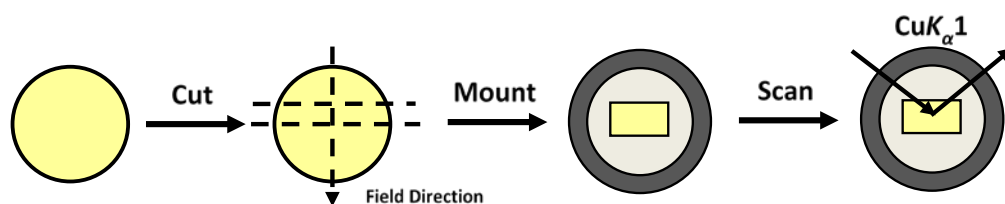
Fig. 4   Cutting and mounting pattern of epoxy pucks cured in magnetic field

The resulting scans were analyzed using Jade 8 software (MDI, Livermore, CA). For each scan, the background was automatically removed, peaks were identified, and pattern fitting was conducted to identify peak area and peak height values in addition to associated errors. The Lotgering factor (LF) was calculated for each scan using the powder diffraction file #01-089-7717 (Synthetic Corundum, space

group $R\bar{3}c$) and Eq. 3. The LF ranges from 0 to 1, with 0 indicating random alignment and 1 indicating perfect alignment.

$$LF = \frac{P_{alignment} - P_{random}}{1 - P_{random}}, \tag{3}$$

where

$$P_{alignment} = \frac{I_{(aligned\ peak)}}{\sum I_{(all)}}, \tag{4}$$

and

$$P_{random} = \frac{I_{(aligned\ peak),PDF}}{\sum I_{(all),PDF}}. \tag{5}$$

According to Eq. 3, $P_{alignment}$ denotes the fraction of the summation of the peak intensities corresponding to the preferred orientation axis to that of the summation of all diffraction peaks in the particle-oriented materials. P_{random} is simply the same as $P_{alignment}$ except calculated from the peak intensities in the powder diffraction file (random orientation). In addition to the LF, synchrotron X-ray powder diffraction and Rietveld refinements were used to calculate the amount of alpha and theta phase alumina in each material.

2.3 Density Functional Theory Calculations

First principles DFT calculations were conducted to provide further understanding of the dopant effect on magnetic alignment and to aid in interpreting the alignment results. The calculations were performed at elevated RE concentrations of $RE_{0.042}Al_{1.958}O_3$ with respect to the experimental composition of $RE_{0.002}Al_{1.998}O_3$. This composition enabled investigating enhanced magnetic properties while maintaining a sufficiently large supercell size to prevent dopant-dopant interactions. Both α- and θ-Al_2O_3 were examined using 120-atom supercells (24 formula units) having lattice vectors on the order of 1 nm. RE-dopants were substituted into an Al^{3+} octahedral site of α- and θ-Al_2O_3 and the additional Al^{3+} tetrahedral site observed in θ-Al_2O_3. Spin-polarized calculations were performed within the Vienna ab initio simulation package using the generalized gradient approximation exchange correlation functional implemented by Perdew-Burke-Ernzerhof and projector augmented wave pseudopotentials.[26–30] A plane-wave cutoff energy of 800 eV was used for the electronic wave function in conjunction with sampling the Brillouin zone with a $2 \times 2 \times 2$ Monkhorst-Pack grid, providing energetic convergence of 0.3 meV/atom. The ion positions and lattice parameters of the RE-doped supercells were optimized to 1 meV/Å. Because the $4f$-electrons in RE sesquioxides have been shown to impact the structural and magnetic properties, they have been considered as valence electrons, except for Yb, which

has a full 4*f*-shell.[31,32] Further model development and computational details may be found in Limmer et al.[33]

Spin-orbit coupled calculations were performed on the optimized RE-doped supercells to determine the doping effect on magnetocrystalline anisotropy energy (MAE) and the easy magnetic axis orientation. These non-self-consistent calculations were performed by manually defining the spin-axis orientation in the crystal and recalculating the system energy. The non-self-consistency prevented spin reorientation to the easy axis during the calculation. The MAE was defined as the change in energy resulting from spin axis reorientation and is indicative of the magnetic anisotropy of the crystal. The minimum energy axis is then designated as the easy axis, and the hard axis corresponds to the maximum energy direction.

3. Results

3.1 Lotgering Factor, Particle Alignment

The (006) and (110) crystal planes were selected to calculated the LF because of their orientations with respect to each other as had been done previously.[12] These 2 planes are perpendicular to each other, which will help gauge if there is alignment in the sample with respect to 2 different alignment directions. Figure 5 illustrates the (006) and (110) crystal planes in a rhombohedral unit cell, such as the unit cell of alumina. Additionally, the (006) crystal plane does not diffract with a large intensity, only 0.6% of the highest intensity peak in alumina. This can often lead to difficulties in data analysis, also prompting the use of the (110) to understand crystal alignment.
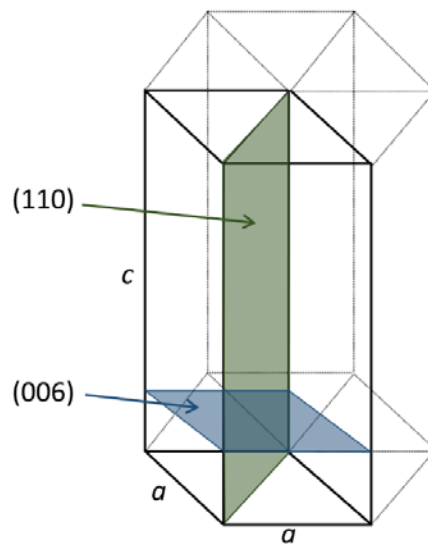

Fig. 5 Idealized rhombohedral unit cell illustrating the (006) and (110) crystal planes

To calculate the LF with respect to the (006) crystal plane, Eqs. 4 and 5 were modified to Eqs. 6 and 7. Similarly, to calculate the LF with respect to the (110) crystal plane, Eqs. 4 and 5 were modified to Eqs. 8 and 9.

$$P_{alignment,(006)} = \frac{I_{(006)}}{I_{(104)}+I_{(006)}+I_{(110)}+I_{(113)}}, \tag{6}$$

$$P_{random,(006)} = \frac{I_{(006),PDF}}{I_{(104),PDF}+I_{(006),PDF}+I_{(110),PDF}+I_{(113),PDF}}, \tag{7}$$

$$P_{alignment,(110)} = \frac{I_{(110)}}{I_{(104)}+I_{(006)}+I_{(110)}+I_{(113)}}, \tag{8}$$

$$P_{random,(110)} = \frac{I_{(110),PDF}}{I_{(104),PDF}+I_{(006),PDF}+I_{(110),PDF}+I_{(113),PDF}}. \tag{9}$$

The calculated LFs for each condition are listed in Table 1. Figure 6 compares alignment for each dopant series with increasing magnetic field with each crystal plane's alignment separated. Er:Al$_2$O$_3$ was not tested for alignment in a 9-T field. Figure 7 shows the XRD spectra obtained from the Yb:Al$_2$O$_3$ samples aligned at 0, 1.8, and 9 T. In the figure, each of the crystal planes are marked which were used for the LF calculations described earlier. The (006) is not present in the 0-T pattern; however, the (006) does appear as the particles align under an increasing magnetic field strength.

Table 1 LFs calculated from (006) and (110) planes for magnetically aligned ceramic composite samples

Composition	LF (%)					
	0 T		1.8 T		9 T	
	(006)	(110)	(006)	(110)	(006)	(110)
Gd: Al$_2$O$_3$	0.25	2.78	27.0	10.0	25.0	10.7
Yb: Al$_2$O$_3$	3.29	2.39	26.6	9.98	51.8	11.2
Pr: Al$_2$O$_3$	0.25	2.93	0.25	2.10	0.25	28.3
Er: Al$_2$O$_3$	10.1	2.65	31.0	12.3	. . .	. . .
Undoped Al$_2$O$_3$	0.25	2.75	0.25	3.01	7.51	8.9
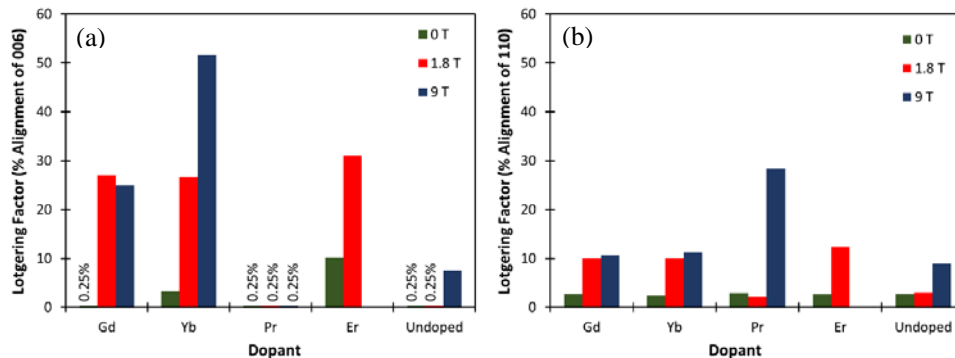
Fig. 6 a) LF as a function of field strength and dopant type with respect to the (006), LF$_{(006)}$ and b) LF as a function of field strength and dopant type with respect to the (110), LF$_{(110)}$
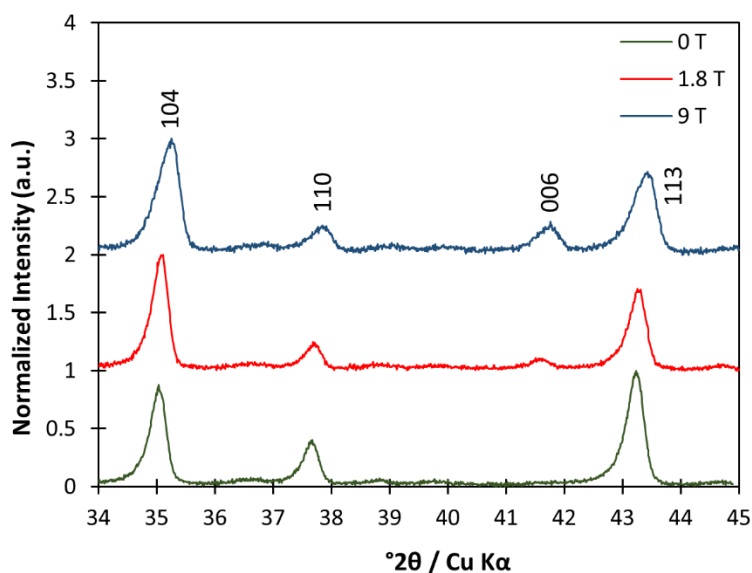
Fig. 7 XRD example spectra of Yb:Al$_2$O$_3$ samples with increasing magnetic field strength

The XRD data for LF$_{(006)}$ shows 3 compositions with significant alignment: Gd:Al$_2$O$_3$, Er:Al$_2$O$_3$, and Yb:Al$_2$O$_3$. Pr:Al$_2$O$_3$ and undoped Al$_2$O$_3$ did not show significant (006) peak intensity to calculate the LF. However, after a 9-T field was applied to the undoped Al$_2$O$_3$, there was a large enough peak to calculate the LF. The XRD data for LF$_{(110)}$ shows essentially the opposite result, with Pr:Al$_2$O$_3$ showing the largest alignment along the (110) plane. The other compositions had comparable orientations, but all were higher than the samples cured without a magnetic field applied.

3.2 DFT Calculated Magnetic Properties

DFT calculations were used to predict the internal magnetic moment of the RE-doped alumina. The magnetic moment magnitude and localization was generally unaffected by the phase and substitution site coordination. However, the magnetic moment increased with an increasing number of unpaired electrons, as shown in Fig. 8. $Gd:Al_2O_3$ had the largest intrinsic magnetic moment (6.9 μ_b), whereas $Yb:Al_2O_3$ had the smallest (0.9 μ_b). The localization of the magnetic moment was considered by examining the magnetic moment isolated to the RE-dopant site, as defined by the Wigner-Seitz radii in the pseudopotential. The magnetic moment is strongly localized to the substitution site for Er, Gd, and Pr with greater than 97% of the magnetic moment localized to the RE-dopant. In contrast, $Yb:Al_2O_3$ showed a large delocalization of the magnetic moment with only 9% of the moment localized on the dopant. The remainder of the magnetic moment was distributed over the surrounding O-atoms such that 83% of the O-atoms in the supercell had an induced magnetic moment.[33]
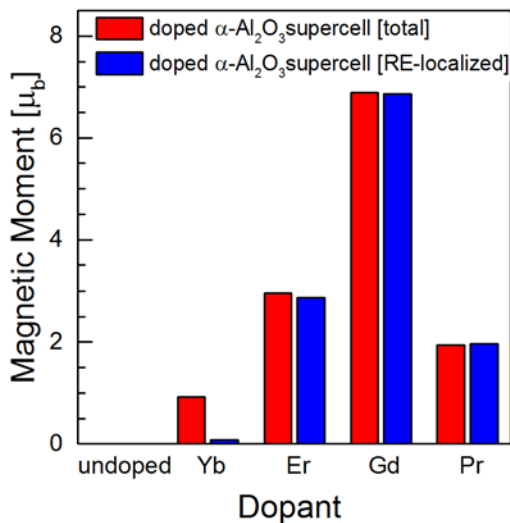
Fig. 8   Intrinsic magnetic moment of RE-doped α-Al₂O₃ indicating the degree of localization around the RE-dopant

The MAE and easy axis were affected by the dopant site and phase as shown in Table 2, though the total magnetic moment remained consistent for a given dopant type. The largest anisotropy was generally observed for Er followed by Pr, with Gd having the smallest anisotropy despite having the largest magnetic moment. θ-Al₂O₃ was more magnetically anisotropic than α-Al₂O₃, and this effect was most

11

pronounced for Pr:Al_2O_3, which had a 3-fold increase in MAE. Additionally, the easy axis was dependent on the dopant type. In α-Al_2O_3, both Gd and Yb maintained easy axes near to easy axis of undoped α-Al_2O_3, the c-axis.

Table 2   DFT calculated easy magnetic axis and maximal MAE (meV) indicating degree of magnetic anisotropy in the RE-doped supercell for RE-dopants in the Al-octahedral site of α- and θ-Al_2O_3

Phase	Composition			
	Yb:Al_2O_3	Er:Al_2O_3	Gd:Al_2O_3	Pr:Al_2O_3
α-Al_2O_3	< 3 2 10 >	< 1 2 0 >	< 0 0 1 >	< 2 3 2 >
	6.1	23.1	0.4	11.0
θ-Al_2O_3	< 3 0 1 >	< -4 3 4 >	< 1 0 20 >	< 1 0 0 >
	0.5	31.3	0.4	30.9

4.   Discussion

The alignment of the doped alumina may be limited by several factors. First, the viscosity of the epoxy could be increasing too quickly for significant particle alignment to occur. If that were the case, one would still expect better alignment with the 9-T field conditions because increasing the magnetic field would decrease the amount of time necessary for alignment. However, not all the samples show increased magnetic alignment. From 1.8 to 9 T, for example, the Gd-doped alumina specimen did not show improved orientation upon alignment under 9 T. This could indicate a maximum field strength exists for particle alignment in this system. Another potential explanation is that steric interactions are hindering particle rotation. This is something that has been reported with other attempts to produce micro-texture. For example, when trying to magnetically align platelet alumina; once the plates come close together, they start to inhibit each other from alignment by impinging each other.[9] Because the powders used in these studies were derived from a chemical precipitation process, it is likely that the particles are not smooth and spherical increasing the likelihood of strong inter-particle interactions that can potentially inhibit alignment. However, since the samples contained only 20-wt% solids, it is unlikely that steric hindrance had a large effect.

The overall agglomeration of alumina crystallites could also be leading to the variation in the data. Although no analysis has been done to quantify the degree of agglomeration, it is likely that some amount of agglomeration was present since no dispersant was used. If multiple crystallites were present in different orientations within the agglomerates, the torques applied to the agglomerate by the magnetic field would be in competition. It is unknown if these torques would be strong enough to break up a soft agglomerate but is unlikely to break up hard agglomerates.

As can be seen in Fig. 6, alignment generally increases with magnetic field strength. Looking at the data, 2 surprising points stand out. The first is both the $Gd:Al_2O_3$ and the $Yb:Al_2O_3$ have similar alignment along the (110) plane despite $Gd:Al_2O_3$ having a much stronger total magnetic moment. However, when considering the $LF_{(006)}$, the $Yb:Al_2O_3$ has a larger response. This may be in part due to the localization of the magnetic moment. In the case of $Gd:Al_2O_3$ the magnetic moment is localized to the dopant position, whereas for $Yb:Al_2O_3$ the magnetic moment is more globally distributed within the structure, possibly inducing higher torque along selected crystal planes for the same field strength. The second interesting result is that the undoped samples experience a small degree of alignment when the field strength is high enough. Calculations indicate a field of approximately 10 T should be necessary for moderate amounts of alignment.[14,17] While this was expected due to the fact that Eqs. 1 and 2 state that no matter how small the magnetic susceptibility anisotropy, if the field strength is strong enough alignment should be possible.

The disproportionately weak response observed in the $Pr:Al_2O_3$ compared with the other dopants is puzzling; increasing the sample size of that condition would be necessary to confirm that the observation is not simply an artifact. If the observation is authentic, it could be explained by differences in magnetic anisotropy between alpha and theta alumina since confirming powder phase showed additional peaks associated with θ-alumina in the $Pr:Al_2O_3$ powder. Table 3 shows the calculated amount of alpha and theta phases in each of the RE-doped alumina materials. The plain alumina was found to be η-alumina, which has a space group of $Fd\overline{3}m$. It is unclear why the plain alumina crystallized as η-alumina which will be explored in another study. Theta and alpha alumina have different behavior to magnetic fields, as predicted by the MAE calculations in Table 2. It is possible that the large amount of theta alumina in $Pr:Al_2O_3$ is the cause of preferred alignment along the (110).

Table 3 Quantification of alumina polymorphs in the materials examined, determined by Rietveld refinement of synchrotron XRD

Composition	Polymorph (%)		
	α	θ	η
Al_2O_3	. . .	. . .	100
$Gd:Al_2O_3$	76	24	. . .
$Yb:Al_2O_3$	84.4	15.6	. . .
$Pr:Al_2O_3$	32.5	67.5	. . .
$Er:Al_2O_3$	62.6	37.4	. . .

The DFT results indicated that the magnetic anisotropy of alpha-phase $Pr:Al_2O_3$ is second only to $Er:Al_2O_3$ for which no experimental result exists for comparison at 9 T. Further, this anisotropy was greatly increased for Pr in θ-Al_2O_3 in comparison

to the alpha phase. Additionally, earlier DFT results showed that increasing the dopant radii increased the relative stability of θ-Al_2O_3, potentially increasing the θ-Al_2O_3 content of the Pr-doped sample more than for the other dopants.[33] This could result in crystals aligning along different directions since the DFT results suggests that doped theta and alpha alumina have different magnetic anisotropy. Preliminary DFT results predict that both Er and Pr shifted the easy axis from the c-axis, the known easy axis for α-alumina[5,12–14,17] suggesting that the (006) peak is no longer the ideal plane to calculate LF. This is confirmed by calculating the LF of the (110) plane, which does show significant alignment in Pr:Al_2O_3.

5.   Conclusions

The experimental results reported here show that magnetic fields can be used to produce particle alignment in alumina. Furthermore, they show the dopant identity affects the responsiveness of alumina to a magnetic field, suggesting a change in the magnetic anisotropy of the crystal that is supported by modeling results. The results also show varying responses from different RE dopants and that in particular Er, Yb, and Gd are particularly effective. There may also be some alumina phase/structural dependency on the alignment as evidenced by preliminary DFT calculations. Gel-casting of alumina parts appears to be a feasible method of inducing particle alignment under an applied magnetic field. Future research will repeat these studies as necessary to determine the effects of the alumina structure on magnetic alignment behavior by calcination to pure alpha and pure theta phases as necessary.

6. References

1. Apetz R, van Bruggen MPB. Transparent alumina: a light-scattering model. Journal of the American Ceramic Society. 2003;86(3):480–486.

2. Hayashi K, Kobayashi O, Toyoda S, Morinaga K. Transmission optical properties of polycrystalline alumina with submicron grains. Materials Transactions. 1991;32(11):1024–1029.

3. Krell A, Klimke J, Hutzler T. Transparent compact ceramics: inherent physical issues. Optical Materials. 2009;31(8):1144–1150.

4. Mata-Osoro G, Moya JS, Pecharroman C. Transparent alumina by vacuum sintering. Journal of the European Ceramic Society. 2012;32(11):2925–2933.

5. Liu P, Yi HL, Zhou GH, Zhang J, Wang SW. HIP and pressureless sintering of transparent alumina shaped by magnetic field assisted slip casting. Optical Materials Express. 2015;5(2):441–446.

6. Krell A, Blank P, Ma H, Hutzler T, van Bruggen M, Apetz R. Transparent sintered corundum with high hardness and strength. Journal of the American Ceramic Society. 2003;86(1):12–18.

7. Liu W, Xie Z, Liu G, Yang, X. Novel preparation of translucent alumina ceramics induced by doping additives via chemical precipitation method. Journal of the American Ceramic Society. 2011;94:3211–3215.

8. Sanamyan T, Pavlacka R, Gilde G, Dubinskii M. Spectroscopic properties of Er^{3+}-doped α-Al_2O_3. Optical Materials. 2013;35(5):821–826.

9. Libanori R, Erb RM, Studart AR. Mechanics of platelet-reinforced composites assembled using mechanical and magnetic stimuli. ACS Applied Materials & Interfaces. 2013;5(21):10794–10805.

10. Libanori R, Reusch FB, Erb RM, Studart AR. Ultrahigh magnetically responsive microplatelets with tunable fluorescence emission. Langmuir. 2013;29(47):14674–14680.

11. Sun ZHI, Guo X, Vleugels J, Van der Biest O, Blanpain B. Alignment of weakly magnetic metals during solidification in a strong magnetic field. Journal of Alloys and Compounds. 2013;551:568–577.

12. Suzuki TS, Sakka Y, Kitazawa K. Orientation amplification of alumina by colloidal filtration in a strong magnetic field and sintering. Advanced Engineering Materials. 2001;3(7):490–492.

13. Terada N, Suzuki HS, Suzuki TS, Kitazawa H, Sakka Y, Kaneko K, Metok N. In situ neutron diffraction study of aligning of crystal orientation in diamagnetic ceramics under magnetic fields. Applied Physics Letters. 2008;92(11):3.

14. Terada N, Suzuki HS, Suzuki TS, Kitazawa H, Sakka Y, Kaneko K, Metoki N. Neutron diffraction texture analysis for alpha-Al2O3 oriented by high magnetic field and sintering. Journal of Physics D-Applied Physics. 2009;42(10):5.

15. Wei M, Zhi D, Brandon DG. Microstructure and texture evolution in gel-cast α-alumina/alumina platelet ceramic composites. Scripta Materialia. 2005;53(12):1327–1332.

16. Yang Z, Yu J, Deng K, Lan L, Wang H, Ren Z, Wang Q, Dai Y, Wang H. Fabrication of textured Si_3N_4 ceramics with β-Si_3N_4 powders as raw material by gel-casting under strong magnetic field. Materials Letters. 2014;135:218–221.

17. Zhang L, Vleugels J, Van der Biest O. Slip casting of alumina suspensions in a strong magnetic field. Journal of the American Ceramic Society. 2010;93(10):3148–3152.

18. Sun ZHI, Zhang X, Pandelaers L, Vleugels J, Van der Biest O, Van Reusel K, Blanpain B. Strong magnetic field effects on solid–liquid and particle–particle interactions during the processing of a conducting liquid containing non-conducting particles. Journal of Colloid and Interface Science. 2012;375(1):203–212.

19. Makiya A, Shouji D, Tanaka S, Uchida N, Kimura T, Uematsu K. Grain oriented microstructure made in high magnetic field. Key Engineering Materials. 2002;206–213:445–448.

20. Sun ZHI, Guo M, Vleugels J, Van der Biest O, Blanpain B. Strong static magnetic field processing of metallic materials: a review. Current Opinion in Solid State and Materials Science. 2012;16(5):254–267.

21. Gillon P. Uses of intense d.c. magnetic fields in materials processing. Materials Science and Engineering: A. 2000;287(2):146–152.

22. Schenck JF. The role of magnetic susceptibility in magnetic resonance imaging: MRI magnetic compatibility of the first and second kinds. Medical Physics. 1996;23(6):36.

23. Sugiyama T, Tahashi M, Sassa K, Asai S. The control of crystal orientation in non-magnetic metals by imposition of a high magnetic field. ISIJ International. 2003;43(6):855–861.

24. Terada N, Suzuki HS, Suzuki TS, Kitazawa H, Sakka Y, Kaneko K, Metoki N. Neutron diffraction texture analysis for α-Al 2 O 3 oriented by high magnetic field and sintering. Journal of Physics D: Applied Physics. 2009;42(10):105404.

25. Park CW, Yoon DY. Effects of SiO2, CaO2, and MgO additions on the grain growth of alumina. Journal of the American Ceramic Society. 2000;83(10):2605–2609.

26. Kresse G, Furthmüller J. Efficiency of ab-initio total energy calculations for metals and semiconductors using a plane-wave basis set. Computational Materials Science. 1996;6(1):15–50.

27. Kresse G, Furthmüller J. Efficient iterative schemes for ab initio total-energy calculations using a plane-wave basis set. Physical Review B. 1996;54(16):11169–11186.

28. Kresse G, Hafner J. Ab initio molecular dynamics for liquid metals. Physical Review B. 1993;47(1):558–561.

29. Kresse G, Joubert D. From ultrasoft pseudopotentials to the projector augmented-wave method. Physical Review B. 1999;59(3):1758–1775.

30. Perdew JP, Ernzerhof M, Burke K. Rationale for mixing exact exchange with density functional approximations. The Journal of Chemical Physics. 1996;105(22):9982–9985.

31. Adachi G, Imanaka N, Kang ZC. Binary rare earth oxides. Vol. 4. Berlin (Germany): Springer Science and Business Media; 2004.

32. Alaan US, Shafer P, Arenholz E, Suzuki Y. Gd-doped BaSnO3: A transparent conducting oxide with localized magnetic moments. Applied Physics Letters. 2016;108(4):042106.

33. Limmer KR, Neupane MR, Brennan RE, Chantawansri TL. Rare-earth dopant effects on the structural, energetic, and magnetic properties of alumina from first principles. Journal of the American Ceramic Society. Paper submitted for publication in 2016.

List of Symbols, Abbreviations, and Acronyms

ARL   US Army Research Laboratory

DFT   density functional theory

DI   deionized

Er   erbium

Gd   gadolinium

LF   Lotgering factor

MAE   magnetocrystalline anisotropy energy

Pr   praseodymium

XRD   X-ray diffraction

Yb   ytterbium

1	DEFENSE TECHNICAL
(PDF)	INFORMATION CTR
	DTIC OCA

2	DIRECTOR
(PDF)	US ARMY RESEARCH LAB
	RDRL CIO LL
	IMAL HRA MAIL & RECORDS
	MGMT

| 1 | GOVT PRINTG OFC |
| (PDF) | A MALHOTRA |

15 DIR USARL
(PDF) RDRL SE
  M WRABACK
RDRL SEE
  G L WOOD
RDRL WML B
  R PESCE-RODRIGUEZ
  B RICE
RDRL WM
  B FORCH
  J ZABINSKI
  M J ZOLTOSKI
RDRL WMM
  M R VANLANDINGHAM
RDRL WMM D
  R H CARTER
RDRL WMM E
  C MOOREHEAD
  J P SINGH
RDRL WMM F
  S M GRENDAHL
  M A TSCHOPP
RDRL WMM G
  J ANDZELM
RDRL WMP C
  R BECKER

INTENTIONALLY LEFT BLANK.